THE ASTROPHYSICAL JOURNAL, 380:564–574, 1991 October 20

PREDICTED EXTREME-ULTRAVIOLET LINE EMISSION FOR NEARBY MAIN-SEQUENCE B STARS

J. J. MACFARLANE[1] AND J. P. CASSINELLI[1]
Department of Astronomy, University of Wisconsin, Madison

B. Y. WELSH, P. W. VEDDER, AND J. V. VALLERGA
Center for EUV Astrophysics, Space Sciences Laboratory, University of California, Berkeley, CA 94720

AND

W. L. WALDRON
Applied Research Corporation, 8201 Corporate Drive, Suite 920, Landover, MD 20785
Received 1990 December 18; accepted 1991 April 26

ABSTRACT

The source of the X-ray emission from O and B stars is currently the subject of debate. Shocks propagating through the winds of O and B stars have previously been proposed to explain their observed X-ray luminosities. Strong shocks with velocity jumps of several hundred km s^{-1} can heat portions of the wind to 10^6–10^7 K, producing major sources of X-ray and extreme-ultraviolet (EUV) emission lines. Alternatively, a corona at the base of the wind might also be responsible for the X-ray emission. In this paper, we investigate the characteristics of EUV lines produced in high-temperature X-ray emitting regions of early B stars. We present estimates of EUV spectral line fluxes for single- and multitemperature plasma models for three nearby main-sequence B stars (β CMa, α Vir, and β Cen A). The plasma models are constrained by X-ray spectral data, and are based on insights from previous hydrodynamics calculations of shocks propagating through hot star winds. The purpose of this paper is to demonstrate the importance of EUV emission lines in determining the properties of the X-ray emitting regions of hot stars. We also show that EUV emission lines from B stars with low interstellar medium hydrogen column densities may be detectable with the moderate-resolution ($\lambda/\Delta\lambda \approx 300$) spectrometers of the *Extreme Ultraviolet Explorer* (*EUVE*) satellite. We investigate the effects of Doppler spreading and the time-dependent attenuation of the overlying wind on line profiles, and discuss how spectral observations can be used to determine temperatures, velocities, and locations of the emitting plasma, thereby providing important insights into the physical processes occurring in extended atmospheres of hot stars.

Subject headings: shock waves — stars: early-type — stars: emission-line — stars: winds — ultraviolet: spectra

1. INTRODUCTION

Stars of spectral class O and early B have been observed to have X-ray luminosities of $\sim 10^{-8}$–10^{-6} times their bolometric luminosity (Harden et al. 1979; Long & White 1980; Cassinelli et al. 1981). Variabilities of up to 30% in the X-ray fluxes have been observed, with time scales ranging from minutes to days (Collura et al. 1989). Most of the X-ray emission appears to originate in hot gas with temperatures of several million degrees. Observations with the *Einstein* Solid State Spectrometer (SSS) also provide evidence for a harder X-ray component, which can be interpreted as arising in a gas with temperatures $\gtrsim 10^7$ K (Cassinelli & Swank 1983; Swank 1985). More recently, it has been proposed (Chen & White 1991) that hard X-rays with photon energies $\gtrsim 2$ keV, and perhaps even γ-emission (Pollack 1987), could be produced by UV photons being scattered by relativistic electrons which are accelerated by shocks in hot star winds.

The source of X-ray emission from early-type stars is not currently well-understood. Some of the X-ray emission could possibly be due to a hot corona at the base of the wind (Cassinelli & Olson 1979; Waldron 1984). Such a corona would have to be very thin to be consistent with the minimal levels of infrared excess observed with the *IRAS* satellite (Lamers, Waters, & Wesselius 1984; Wolfire, Waldron, & Cassinelli 1985). However, there are at least two pieces of evidence that suggest the X-rays are not solely due to coronae. Firstly, there appears to be too little attenuation of soft X-rays (with energies between 0.6 and 1.0 keV) by the overlying wind for a corona to be the source of all of the X-rays (Cassinelli et al. 1981). Secondly, there has been no detection of optical coronal lines (e.g., Fe XIV at 5303 Å) that might be expected for a coronal plasma (Nordsieck, Cassinelli, & Anderson 1981; Baade & Lucy 1987). Since the fluid velocity of coronal regions is small and Doppler shifts are minimal, these coronal lines should be much more readily observable than similar lines emitted from shock-heated regions.

Early-type stars also show strong ultraviolet resonance lines for "superionization" stages such as O VI, N V, and C IV (Lamers & Morton 1976; Lamers, Gathier, & Snow 1980). The presence of these ionization stages in early O star winds might be due to radiative transfer effects (Pauldrach et al. 1987), while in later O and B stars they are probably produced through the Auger process by the X-ray radiation field. The UV resonance lines exhibit broad P Cygni profiles, indicating that these stars are losing mass at large rates through dense, high-velocity winds (Lamers & Morton 1976), with maximum wind speeds being roughly 3 times the star's escape velocity (Lamers, van de

[1] Postal address: Washburn Observatory, University of Wisconsin, 475 North Charter Street, Madison, WI 53706.

Heuvel, & Petterson 1976; Snow & Morton 1976). Analyses of observed P Cygni profiles of O stars (Groenewegen, Lamers, & Pauldrach 1989) find that the shapes of the violet absorption wings and the wavelengths of the emission peaks can be better reproduced with a model which includes the effects of "turbulence" in the wind (i.e., wind velocity profiles which are not monotonically increasing). Such "turbulence" could be consistent with shocks forming in the winds. Superposed on the P Cygni profiles are narrow absorption components (NACs) (Lamers, Gathier, & Snow 1982) which suggests that the winds have abrupt changes in density. These features occur at velocities that are a few hundred km s^{-1} below the observed maximum wind velocities. Shocks with velocity jumps of this magnitude produce plasmas with temperatures $\sim 10^6$–10^7 K and can produce emission consistent with observed X-ray spectra (MacFarlane & Cassinelli 1989, hereafter MC). Recent observations of the time-variability of NACs suggest that their evolution is systematic (Prinja, Howarth, & Henrichs 1987; Henrichs, Kaper, & Zwarthoed 1988; Kaper et al. 1989) with changes occurring over time scales of tens of hours. Henrichs et al. (1988) and Prinja (1988) have shown there is a correlation between stellar rotation period and the appearance and evolution of NACs for several O stars.

While our understanding of high energy phenomena in hot stars has improved significantly over the past 10 to 15 years, much of the observational information has come from rather low spectral resolution data such as from *Einstein* X-ray spectrometers, broad-band *IRAS* fluxes, and radio continuum observations. Direct observation of spectral emission lines would provide significant new constraints for deducing the properties of the extended regions of hot star winds. The first opportunity to obtain line emission spectra of the X-ray/EUV emitting regions will come with the launch of the *Extreme Ultraviolet Explorer* (*EUVE*) satellite. The medium-resolution spectral capability of *EUVE* (Bowyer & Malina 1991) will present important opportunities for deducing the location and characteristics of the X-ray emission from nearby hot stars.

Recently, Cassinelli et al. (1991) have shown that the nature of the X-ray emission from early B stars may be revealed through observations with *EUVE*. The purpose of the present paper is to predict in greater detail the characteristics of EUV line emission for three nearby early-type stars, and to illustrate how such data will help constrain models of hot star X-ray sources. The best candidates for observation are nearby early B stars that have low interstellar medium (ISM) column densities and are known X-ray emitters. There is significant absorption by interstellar H and He at wavelengths from 912 down to about 100 Å. Because O stars tend to be at large distances and have large neutral hydrogen column densities, it is likely that only nearby B stars with low ISM column densities will be detected by *EUVE*.

The organization of this paper is as follows. In § 2, we briefly review the shock model of MC that was used to study the properties of shocks propagating through the wind of τ Sco (B0 V). We shall use this model as a basis for our discussions for the shocked X-ray emitting regions of β CMa (B1 II–III), α Vir (B1 IV), and β Cen A (B1 III). In § 3, we present results of calculated line profiles from coronal and shock models. We also examine the effect of Doppler spreading of emission lines in high-velocity winds and the effects of attenuation by the overlying "cool" wind. In § 4, we use observational constraints from the *Einstein* Imaging Proportional Counter (IPC) data and insights from our shock model to predict EUV emission-line fluxes. These model fluxes are then folded through the *EUVE* spectrometer response functions and predicted spectra are shown. In § 5, we present an overall review of this investigation.

2. SHOCK-PRODUCED X-RAYS IN HOT STAR WINDS

Hot stars are known to have dense, high velocity winds (Snow & Morton 1976) that are losing mass at rates $\sim 10^{-8}$–$10^{-5}\ M_\odot\ yr^{-1}$ (Gathier, Lamers, & Snow 1981). The winds are driven by the scattering and absorption of photospheric radiation by spectral lines (Lucy & Solomon 1970; Castor, Abbott, & Klein 1975). Lucy (1982) argued that line-driven stellar winds are unstable and that perturbations in the flow velocity grow into a series of shocks. Predictions from his model are not in detailed agreement with observations because the shocks tend to be too weak. Calculations by Owocki, Castor, & Rybicki (1988, hereafter OCR) suggest that instabilities may produce strong shocks that are capable of heating portions of the wind to several million degrees. Their time-dependent radiation-hydrodynamics calculations, which ultilize a line-driving model based on pure absorption, suggest that instabilities can produce a highly structured wind with approximately 10 shocks within about 2 stellar radii that propagate outward through the wind. More recently, Owocki (1991) has performed calculations using a model which includes the effects of scattering and found that, while the diffuse radiation drastically reduces the intrinsic (nonperturbed) variability of the wind, the winds remain advectively unstable to perturbations $\gtrsim 1\%$.

Recently, MC performed time-dependent hydrodynamics calculations for early B stars. Using a phenomenological radiative acceleration model, they showed that the *Einstein* SSS X-ray observation for the early B star τ Sco is consistent with strong shocks propagating through its wind. In a sense, the calculations of OCR and MC were complementary because while OCR studied the *formation* process of multiple shocks in isothermal winds; MC investigated the temperature structure, influences of radiative cooling and electron conduction, and X-ray emission properties of a single shock propagating through a model wind. In both calculations, the shock-heated X-ray emitting region is characterized by a strong reverse (starward-facing) shock which forms as a relatively cool, high-velocity portion of the wind rams into the slower moving, hot material ahead of it. Typical results from the MC model are schematically illustrated in Figure 1, where the wind temperature, velocity, and density are shown as a function of position. The temperature increases abruptly to $\gtrsim 10^6$ K for both the forward and reverse shock fronts, while the density increases by a factor of 4. The position of the shock-heated region is of course time-dependent because material continually flows away from the star. At some later time, another shock forms and propagates through the wind and the process repeats itself.

The point we wish to emphasize here is that the velocity of the high-temperature, X-ray emitting region does *not* correspond to the terminal velocity (v_∞) associated with UV observations. This velocity is determined from the P-Cygni profiles of ions that are present in the cool wind. In contrast, the X-ray emitting region moves at a velocity that is several hundred km s^{-1} slower than the cool wind on the starward side of the reverse shock. This is an important point because it may be possible to observe both emission lines from the X-ray emitting

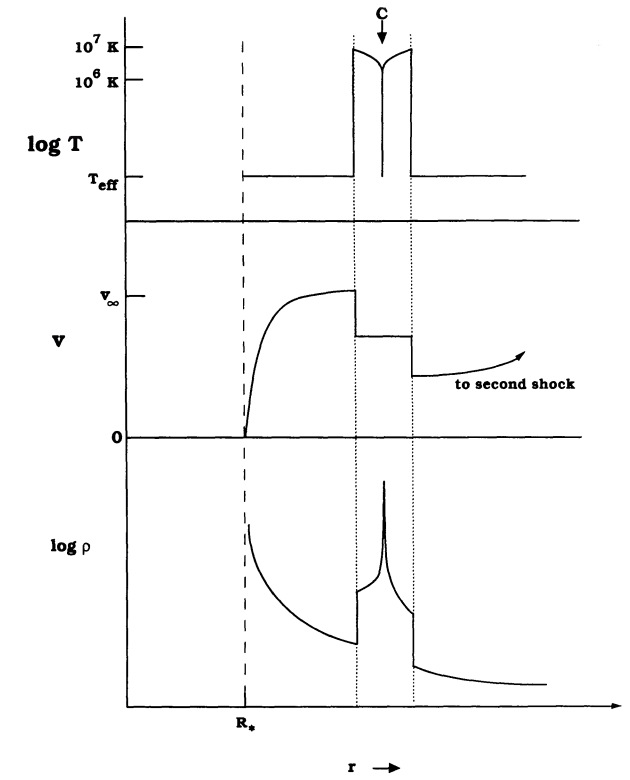

FIG. 1.—Schematic illustration of with temperature, velocity, and density distributions in a shock-heated wind. Label "C" indicates the locations of the "contact region." Note that the velocity of the high-temperature region is several hundred km s^{-1} lower than the maximum velocity of the cooler region.

region (Cassinelli et al. 1991), and cool wind absorption lines at wavelengths above the He I edge at 504 Å (Kudritzki 1991).

An open question associated with X-ray producing shocks in hot star winds is the rate at which shocks form. The calculations of OCR suggest that shocks form as a result of instabilities on time scales of $\sim 10^3$ s. However, Mullan (1984) suggested that shocks form at the surfaces of "corotating interaction regions" as a result of stars emitting winds in a nonspherically symmetric manner (see Fig. 2). In this senario, the hot X-ray emitting region is spiral-shaped, and is bounded by a

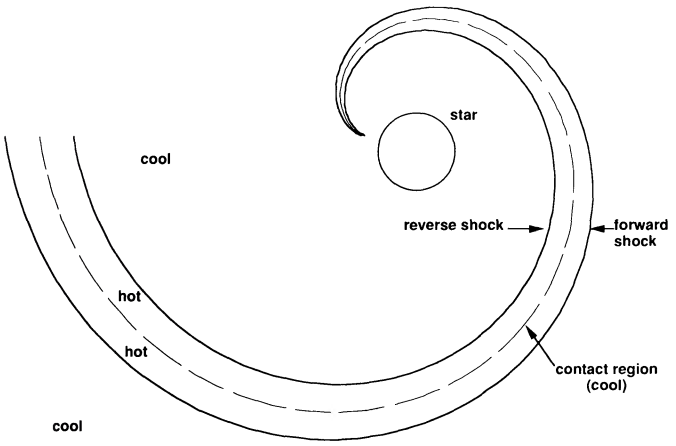

FIG. 2.—Schematic illustration of the forward/reverse shock pairs that form in a corotating interaction region. The location of contact region is indicated by the dashed line.

forward/reverse shock pair. The shocks continually sweep up the cooler wind material as they propagate in the direction away from the hot region. In this case, shocks form continuously, but a new shock region passes by a given point in space only once every rotation period ($\sim 10^5$ s). This scenario is consistent with the observed correlation of the time-dependence of the NACs and the stellar rotation.

The NACs are probably caused by a large amount of cool ($T \sim 10^4$–10^5 K) material moving within a narrow velocity range. In the shock model illustrated in Figure 1, it seems quite possible that NACs result from attenuation by the high-density, low-temperature region that forms between the forward and reverse shocks, referred to as the "contact region" (labeled as C in Fig. 1). The high-density material near the contact region can cool rapidly to roughly the stellar effective temperature as a result of radiative cooling. The NACs tend to be absent from the P Cygni profiles of stars with lower density winds (Lamers et al. 1982). This may be a result of lower density winds having longer radiative cooling times, or perhaps not enough material near the contact region to produce appreciable attenuation. Although the width of the contact region in Figure 1 is very narrow, the total mass in the region is quite large because of its high density. Thus, the existence of NACs is consistent with shock models which have strong reverse shocks, hot X-ray emitting regions moving a few hundred km s^{-1} slower than the terminal velocity, and cooler dense material moving at roughly the same velocity as the hot material.

3. HIGH-RESOLUTION EXTREME-ULTRAVIOLET EMISSION SPECTRA

The X-ray emission from hot stars indicates the presence of material with mean temperatures of 10^6–10^7 K, with some evidence for material at temperatures above 10^7 K (Cassinelli & Swank 1983; Swank 1985). A significant fraction of the radiation emitted by low-density plasmas at these temperatures can be in the form of discrete lines. For near-solar composition plasmas, high-Z materials such as O, Ne, Si, and Fe are a significant source of line radiation at EUV and X-ray wavelengths. In this section, we present source-dependent emission spectra in the wavelength range from 100–110 Å. This part of the spectrum may provide a good opportunity to deduce the physical properties of X-ray source regions of hot stars because: (1) several strong Fe ions, whose fractional abundance depends strongly on temperature, are present, and (2) attenuation effects are modest at these relatively short EUV wavelengths. The qualitative results of this section can of course be applied to other parts of the EUV spectrum as well.

We will first consider line emission from stationary plasmas, such as would approximately be the case for coronal emission. Later, we investigate the effects of Doppler spreading for shock-heated regions propagating radially outward away from the star. We also examine the case of a hybrid corona-shock model in which lines are emitted both from a stationary plasma at the base of the wind and shock-heated material moving at high speeds. And finally, we examine the effects of attenuation by the overlying cool wind and ISM on the lines.

3.1. *Coronal Line Emission*

Let us consider the radiant emission from a single bound-bound transition with a Doppler line profile. For coronal emission we assume the plasma velocity is small ($v \ll c$). The energy emitted per second per unit frequency can be written as

TABLE 1

ATOMIC DATA OF LINES BETWEEN 100 AND 110 Å

Ion	Wavelength (Å)	Oscillator Strength	Gaunt Factor
Fe XXII	102.40	0.10	0.84
O VIII	102.44	0.08	0.04
Ne VIII	103.10	0.30	0.11
Fe XXI	103.30	0.05	1.00
Fe IX	103.60	0.23	0.20
Fe XVIII	103.90	0.06	0.78
Ni IX	104.00	0.55	0.20
O VI	104.80	0.03	0.45
Fe IX	105.20	0.15	0.20
Ne VII	106.20	0.46	0.05
Fe VIII	108.10	0.24	0.91
Fe XIX	108.40	0.10	0.75

(Mihalas 1978)

$$L_\nu = (8\pi h\nu_0^3/c^2)\int d^3r n_u(g_l/g_u)\alpha_{ul}(\nu)\,, \quad (1)$$

where the integral is over the volume of the emitting region, n_u is the number density of ions in the upper state of the transition, g_l and g_u are the statistical weights of the lower and upper states, respectively, $h\nu_0$ is the transition energy, h is Planck's constant, and c is the speed of light. The bound-bound absorption cross section is

$$\alpha_{ul}(\nu) = (\pi e^2/m_e c)f_{ul}\,\phi_\nu\,, \quad (2)$$

where m_e and e are the electron mass and charge, respectively, and f_{ul} is the oscillator strength. The normalized Doppler profile can be written as

$$\phi_\nu = (1/\pi^{1/2}\Delta\nu_D)\exp(-x^2)\,, \quad (3)$$

where

$$x = (\nu - \nu_0)/\Delta\nu_D \quad \text{and} \quad \int_0^\infty \phi_\nu d\nu = 1\,.$$

The quantity $\Delta\nu_D$ is the thermal Doppler width. The excited state number density, n_u, is determined by steady state detailed balancing arguments. The collisional excitation rate is balanced by the radiative decay rate to give (see, e.g., Tucker & Gould 1966)

$$n_u = \frac{(3.65\times10^{-13}\ \text{cm}^3\ \text{eV}^{7/2})n_l\,n_e(g_u/g_l)g_{ul}\exp(-h\nu/kT)}{(h\nu_0)^3(kT)^{1/2}}\,, \quad (4)$$

where n_l is the number density of lower (ground) state ions, g_{ul} is the Gaunt factor, T is the plasma electron temperature, and k is Boltzmann's constant. Combining equations (1) and (4), we obtain:

$$L_\nu = (2.53\times10^{-17}\ \text{ergs cm}^3\ \text{s}^{-1})\phi_\nu f_{ul}\,g_{ul}f_E \times\int d^3r f_{IZ}\,n_e^2(T_{eV})^{-1/2}\exp(-h\nu/kT)\,, \quad (5)$$

where f_E is the fractional elemental abundance (per free electron), f_{IZ} is ionization abundance, and T_{eV} is the electron temperature in eV. If we assume the temperature of the X-ray emitting region is uniform, the luminosity can be written in terms of the X-ray emission measure ($\text{EM}_x \equiv \int d^3r n_e^2$):

$$L_\nu = (2.53\times10^{-17}\ \text{ergs cm}^3\ \text{s}^{-1})\ \text{EM}_x\,\phi_\nu f_{ul}\,g_{ul} \times f_E f_{IZ}(T_{eV})^{-1/2}\exp(-h\nu/kT)\,. \quad (6)$$

The single line flux seen at the Earth from a star at a distance D is

$$F_\nu = L_\nu/(4\pi D^2)\,. \quad (7)$$

Atomic data for the lines we have considered are listed in Table 1. The transition energies, oscillator strengths, and Gaunt factors are taken from Raymond & Smith (1977). Ionization fractions calculated with the Raymond-Smith code are listed in Table 2 at temperatures, of 1, 2, 4, and 10×10^6 K. We have assumed the same elemental abundances as Raymond & Smith (1977) in computing line fluxes.

The spectral fluxes between 100 and 110 Å for isothermal coronal models for β Cen are shown in Figure 3. Plots (*a*) through (*d*) represent coronal temperatures of 1, 2, 4, and 10×10^6 K, respectively. For each case, we have taken $\text{EM}_x = 4\times10^{53}\ \text{cm}^{-3}$. (We note that the chosen values of EM_x and T are not consistent with the *Einstein* IPC data described in § 4. However, our goal here is to show the relative strengths of the emission lines at various plasmas temperatures.) The contribution to the flux from Bremsstrahlung is included to provide a rough estimate of the magnitude of the continuum.

Figure 3 shows that a variety of strong emission lines are

TABLE 2

IONIZATION FRACTIONS OF SELECTED LINES

Ion	Wavelength (Å)	Ionization Fractions[a]			
		$T = 1\times10^6$ K	$T = 2\times10^6$ K	$T = 4\times10^6$ K	$T = 1\times10^7$ K
Fe XXII	102.40	0	0.21 (−17)	0.95 (−7)	0.10 (0)
O VIII	102.44	0.93 (−2)	0.44 (0)	0.17 (0)	0.16 (−1)
Ne VIII	103.10	0.67 (−1)	0.13 (−1)	0.51 (−2)	0.56 (−4)
Fe XXI	103.30	0	0.50 (−13)	0.82 (−5)	0.19 (0)
Fe IX	103.60	0.35 (0)	0.24 (−3)	0.24 (−9)	0.84 (−17)
Fe XVIII	103.90	0	0.56 (−3)	0.91 (−1)	0.14 (0)
Ni IX	104.00	0.58 (−1)	0.20 (−3)	0.77 (−10)	0.14 (−18)
O VI	104.80	0.54 (−2)	0.24 (−2)	0.96 (−4)	0.61 (−6)
Fe IX	105.20	0.35 (0)	0.24 (−3)	0.24 (−9)	0.84 (−17)
Ne VII	106.20	0.15 (−1)	0.37 (−3)	0.31 (−4)	0.70 (−7)
Fe VIII	108.10	0.79 (−1)	0.12 (−4)	0.35 (−11)	0.29 (−19)
Fe XIX	108.40	0	0.77 (−6)	0.77 (−2)	0.22 (0)

[a] Exponents are in parentheses.

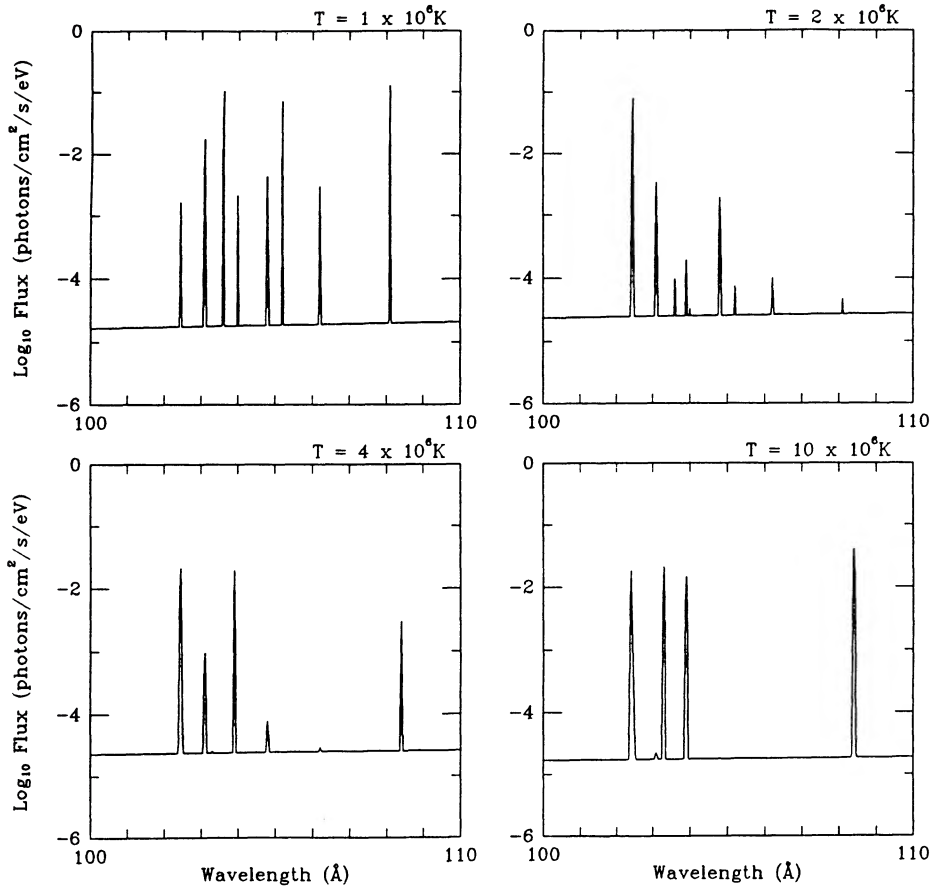

FIG. 3.—Computed line spectral fluxes for isothermal coronal models with plasma temperatures of 1×10^6 K, 2×10^6 K, 4×10^6 K, and 10×10^6 K

present at each temperature. For instance, at 1×10^6 K, Fe VIII (108.1 Å) and Fe IX (103.6 and 105.2 Å) have line center fluxes near 10^{-1} photons cm^{-2} s^{-1} eV^{-1}. This corresponds to frequency-integrated fluxes of 1–2 $\times 10^{-3}$ photons cm^{-2} s^{-1}. At $T = 2 \times 10^6$ K, O VIII (102.44 Å), Ne VIII (103.1 Å), and O VI (104.8 Å) are the strongest lines. At $T = 4$ and 10×10^6 K, higher ionization stages of Fe emit the strongest lines (Fe XXII at 102.4 Å, Fe XVIII at 103.9 Å, and Fe XIX at 108.4 Å). Although the line center fluxes are slightly lower at the higher temperatures, the frequency-integrated fluxes for the strongest lines are again 1–2 $\times 10^{-3}$ photons cm^{-2} s^{-1}. These results show that in this fairly narrow spectral region of the EUV, a variety of ions emit strong lines which can be used to deduce the temperatures of the X-ray emitting regions of hot stars.

3.2. *Line Emission from Shocks*

If the high-temperature X-ray emitting regions are moving rapidly away from the star, the lines will be substantially broadened due to the Doppler effect. Wind velocities for hot stars are often observed to be $\sim$1000–3000 km s^{-1}. Therefore, we might expect line widths at 100 Å to range up to $\Delta\lambda = \lambda\beta \approx \pm 1$ Å ($\beta \equiv v_{\rm wind}/c$). We have computed the spectral luminosity in this case by integrating the line profile over the angle between the observer and the wind velocity vector, $\theta \equiv \cos^{-1}\mu$. For a Doppler profile,

$$L_\nu \propto \int_{-1}^{1} d\mu \exp\left(-[x - \delta\mu]^2\right), \qquad (8)$$

where $\delta = \beta v_0/\Delta v_{\rm D}$. For $\delta \gg 1$, the profile from an optically thin shell is "flat-topped." Thus, the photons from a single line will be distributed almost equally over $\Delta\lambda = \pm\lambda\beta$. For the conditions discussed in this paper, $\delta \sim 10^2$.

The spectral fluxes computed for $\beta = 0.01$ are shown in Figure 4. In these calculations, we used the same emission measures and atomic data as in Figure 3. The lines are seen to be broadened over ± 1 Å. This results in some overlapping between closely spaced lines. By comparison, the resolution of *EUVE* in this range is about 0.3–0.4 Å. This suggests *EUVE* observations may be able to distinguish between coronal and shock EUV/X-ray emitting regions.

We have also computed the spectral flux for a "hybrid model." Many hot stars observed with the *Einstein* Solid State Spectrometer appear to be emitting X-rays from plasmas with temperatures above 10^7 K (Swank 1985). One could speculate that the hard X-rays originate in a corona at the base of the wind, while the softer X-rays are emitted from shocks. Fluxes from this type of model are shown in Figure 5. For these calculations we assumed EM = 1×10^{53} cm^{-3} for each of four isothermal regions with $T = 1$, 2, 4, and 10×10^6 K. The 1, 2, and 4×10^6 K components were assumed to have wind velocities of $\beta = 0.01$, while the 1×10^7 K component was stationary. Figure 5 clearly shows narrow lines from the high-temperature region mixed with the broadened lines from the lower temperature regions. These results demonstrate how EUV line fluxes may allow us to deduce the origin of radiation from relatively complex, multicomponent sources.

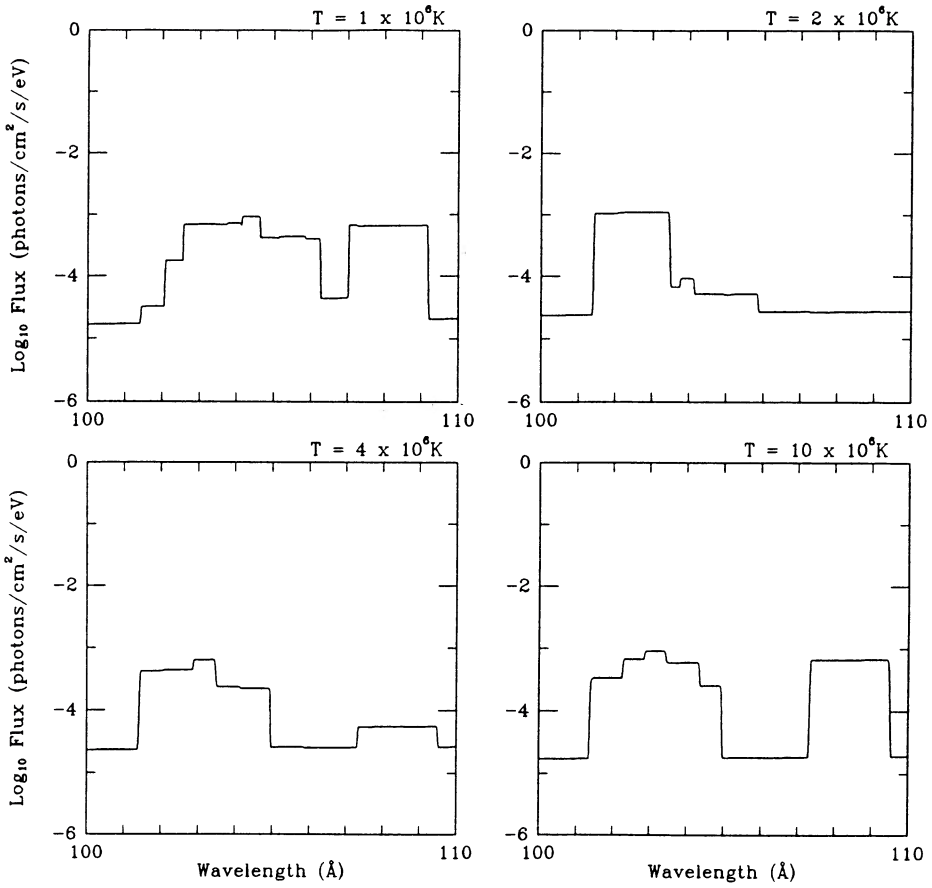

FIG. 4.—Computed line spectral fluxes for isothermal shock models with plasma temperatures of 1×10^6, 2×10^6, 4×10^6, and 10×10^6 K

3.3. *Attenuation Effects*

Emission lines originating in a high-velocity wind have profiles that can be preferentially attenuated in the longward of line center. This is because the redshifted side of a line originates on the far side of the star, and has more absorbing material to travel through. For instance, consider the case illustrated in Figure 6, where a thin, hot, spherically expanding shell emits X-ray and EUV radiation. In the winds of early B stars, the EUV lines can be significantly attenuated by the neutral He. For the simple case where the wind density is given by $n(r) = n_0(R_*/r)^2$, the optical depth from the point of emission to the observer is

$$\tau(v, \theta) = \frac{n_0 R_*}{x_E} f_{He} \alpha_{He}(v) \frac{\theta}{\sin \theta} \equiv \tau_0(v) \frac{\theta}{\sin \theta}, \quad (9)$$

where x_E is the radius of the emitting shell in units of the stellar radius ($x_E = R_E/R_*$), f_{He} is the fractional helium abundance (assumed to be 0.078), $\alpha_{He}(v)$ is the He photoionization cross section, and θ is the angle between the observer and the source. The density distribution assumed above is consistent with a wind where the mass flux is spatially uniform and the velocity is constant.

The frequency-dependent flux can be written as

$$F_v = \frac{\Lambda^L(T)\, EM_x}{4\pi D^2} A_v \exp(-\tau_{ISM}) \quad (10)$$

where

$$A_v = \tfrac{1}{2} \int_{\mu_{min}}^{1} d\mu\, \phi_v \exp\{-\tau_0 \cos^{-1}(\mu)(1-\mu^2)^{-1/2}\}, \quad (11)$$

$$\mu \equiv \cos\theta,$$

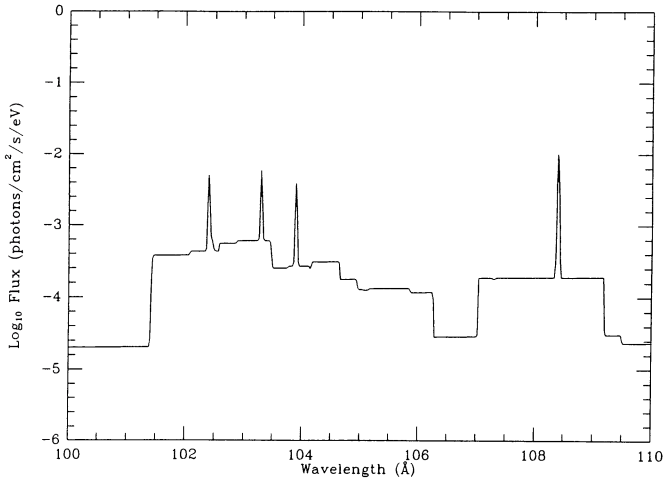

FIG. 5.—Computed line spectral flux for hybrid shock/coronal model. The material at $T = 10 \times 10^6$ K is stationary, while the material at $T = 1$, 2, and 4×10^6 K is moving at $v_{wind} = 0.01c$.

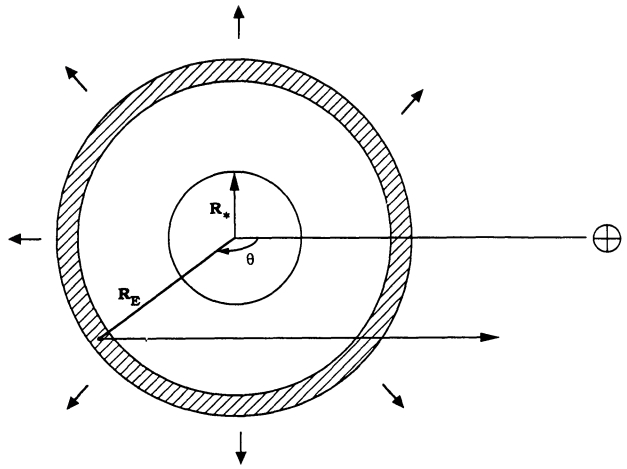

FIG. 6.—Schematic illustration of an X-ray emitting shell expanding away from a star.

and

$$\mu_{\min} \equiv -\sqrt{1 - x_E^{-2}} .$$

The quantity $\Lambda^L(T)$ is the line power coefficient, and τ_{ISM} is the ISM optical depth. The cutoff in equation (11) is due to occulation by the stellar disk. For a line with a Doppler profile, the frequency-dependent attenuated line profile for the overlying wind becomes

$$A_\nu = \frac{1}{2\pi^{1/2}\Delta\nu_D} \int_{\mu_{\min}}^{1} d\mu \exp\left[-(x - \delta\mu)^2 - \tau_0 \frac{\cos^{-1}(\mu)}{\sqrt{1-\mu^2}} \right] . \quad (12)$$

The attenuated line profile is plotted in Figure 7 as a function of wavelength displaced from line center for several values of τ_0. When the overlying wind optical depth is low, the line profile is flat-topped (*top curve*). However, as the wind optical depth increases, the redshifted part of the line ($\Delta\lambda > 0$) becomes significantly more attenuated than the blueshifted portion. The ratio of the redshifted to blueshifted flux decreases as the optical depth increases. Thus, one can attempt to deduce the value of τ_0 ($\propto n_0/x_E$) by measuring the ratio of the redshifted to blueshifted intensities. Lines at 100 and 200 Å would of course have different line profiles because of differing amounts of attenuation.

The variation of τ_0 with wavelength and shock position can be estimated as follows. For a wind with a constant mass flux, the density $\rho = (\dot{M}/4\pi R_*^2 v_\infty)$, where $\dot{M}$ is the mass-loss rate. Using the empirical formula of Kudritzki et al. (1989) for early B stars, we find $\dot{M} \approx 1 \times 10^{-8}$ and $n_0 \approx 2 \times 10^8$ cm^{-3}. For the neutral He cross section, a reasonable fit to the results of Reilman & Manson (1979) between 100 and 504 Å is: $\alpha_{He}(\lambda) = 2.1 \times 10^{-19}$ cm^2 $(\lambda/100\ \text{Å})^{2.3}$. This gives

$$\tau_0(\lambda) \approx \frac{2.0}{x_E} \left(\frac{\lambda}{100\ \text{Å}} \right)^{2.3} . \quad (13)$$

The value of τ_0 is plotted in Figure 8 as a function of wavelength for several values of x_E. For a shock at $50R_*$ (*lower curve*), the optical depth is less than 1 for wavelengths below 400 Å. However, near the star the optical depth of the overlying wind can be large enough to significantly attenuate lines, particularly those with wavelengths >150 Å. If we assume that τ_0 must be less than 1 in order for lines to be observed, only lines below 100 Å would be observed at $2R_*$. As the shock propagates outward, lines up to about 180 Å would be seen at $10R_*$, and lines up to about 370 Å would be seen at $50R_*$. (As a reference, the time it takes a shock travelling at 1500 km s^{-1} to travel $50R_*$ is about 60 hr.) Thus, unless the X-ray sources are very far from the star ($r \gtrsim 100R_*$), we expect each emission line intensity to show a different time-dependence.

Finally, one must consider the attenuation by the interstellar medium. Figure 9 shows the dependence of the ISM attenuation factor [$= \exp(-\tau_{ISM})$] with wavelength for several neutral H column densities. Of the three stars, β CMa has the lowest column density ($<2 \times 10^{18}$ cm^{-2}). For this reason,

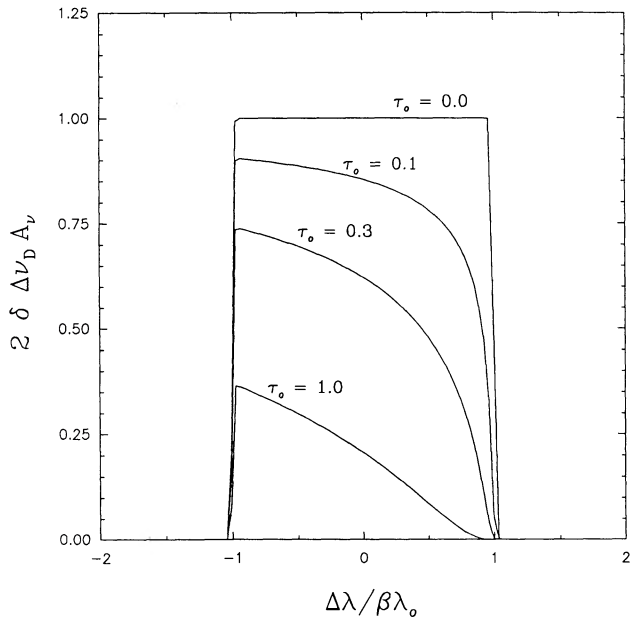

FIG. 7.—Dependence of EUV line profiles on the overlying wind optical depth. The scaled value of the attenuated line profile is plotted as a function of the displacement for line center for several values of τ_0.

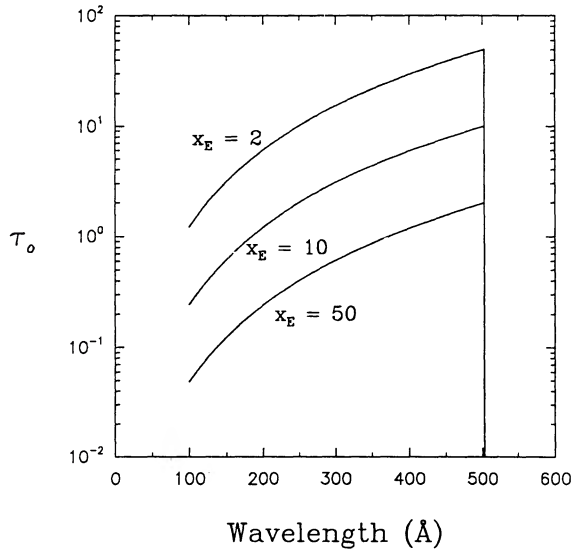

FIG. 8.—Optical depth parameter for the overlying wind as a function of wavelength and the position of X-ray emitting region, $x_E \equiv R_E/R_*$.

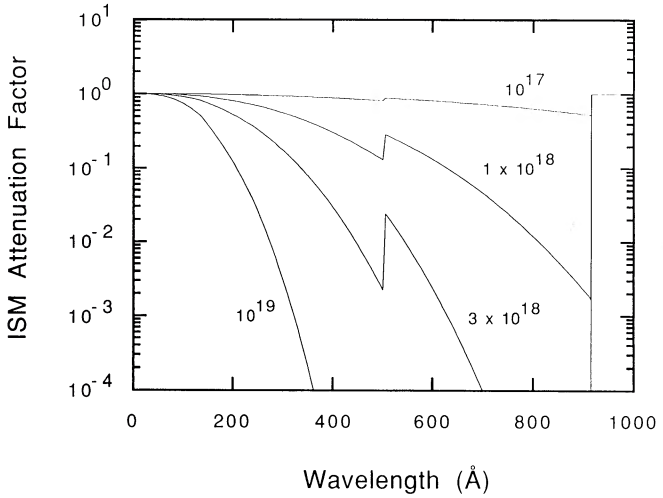

FIG. 9.—Interstellar medium attenuation factor for several values of the column density.

β CMa offers the best opportunity to see emission lines over a wide spectral range. For stars with ISM column densities above 10^{19} cm^{-2}, one would not expect to see emission lines at wavelengths longer than 200–300 Å. For stars with column densities greater that 10^{20} cm^{-2}, detection of EUV emission lines from hot star winds is extremely improbable. Unfortunately, this means that no O stars should be detected with *EUVE*.

4. PREDICTIONS FOR EXTREME-ULTRAVIOLET LINE EMISSION

In this section, we discuss the characteristics of EUV radiation emitted from the extended atmospheres of a few nearby early B stars, and describe how observations with the *EUVE* satellite may provide important information about the properties of hot star X-ray/EUV sources. Some relevant parameters for the three early B stars we consider are listed in Table 3. These particular stars are considered good candidates for detection by *EUVE* because: (1) they are known X-ray sources, having been observed with the *Einstein* Imaging Proportional Counter (IPC) (Agrawal et al. 1984); (2) they are of a spectral type that should have high-velocity winds; and (3) their interstellar medium (ISM) column densities are relatively low.

4.1. *Constraints by IPC Data*

We have computed EUV line fluxes from two widely different types of models that are consistent with IPC X-ray observations to estimate the emission from the stars under consideration. In the first model, we have fitted the observed

TABLE 3

STELLAR PARAMETERS

Star	Spectral Type	Distance (pc)	ISM Column Density (cm^{-2})	IPC Count Rate (counts s^{-1})
β CMa	B1 II–III	203[a]	$<2 \times 10^{18}$ [b]	0.80[c]
α Vir	B1 IV	86[a]	7×10^{18} [b]	0.227[d]
β Cen A	B1 III	81[d]	4×10^{19} [b]	0.183[d]

[a] Shull & Van Steenberg 1985.
[b] Welsh, Vedder, & Vallerga 1990.
[c] Agrawal et al. 1984.
[d] Long & White 1980.

TABLE 4

ISOTHERMAL FITS TO IPC DATA

Star	IPC Bins	$\log_{10} T$ (K)	EM (cm^{-3})	χ^2
β CMa	1–8	6.4	3.0×10^{53}	3.4
α Vir	1–8	6.2	1.1×10^{53}	3.5
β Cen A	1–9	6.3	1.3×10^{53}	5.9

IPC data to a simple isothermal plasma model. The best fits were obtained by adjusting the plasma temperature and the X-ray emission measure. Table 4 lists results for the best-fit cases for each star. The χ^2 values for all three stars show that the fits to the IPC data are reasonably good. We found that variations in the column density by as much as a factor of 5 had little affect on our IPC fits. This is because the wind column density and ISM column densities for these stars are too small to produce any significant attenuation at the C, N, and O photoionization edges between 0.3 and 0.6 keV. Thus, the IPC data does not provide constraints for the ISM and overlying wind column densities for these stars.

For the second model, we consider the case of a plasma with a wide range of temperatures. Hydrodynamics calculations of shocks propagating through model winds for τ Sco (B0 V) typically found temperatures near the shock region to be distributed between about 1 and 10 million degrees (MC). The calculations predicted a more-or-less uniform differential emission measure ($\equiv d\mathrm{EM}/dT$) over this temperature range. The calculated temperature distributions were found to produce an X-ray spectrum very similar to that of the two-temperature best-fit model ($T_1 = 5.3 \times 10^6$ K and $T_2 > 15 \times 10^6$ K) determined from fits to *Einstein* SSS data (Cassinelli 1985). To test whether the X-ray emitting regions of β Cen, α Vir, and β CMa could be due to plasmas with a wide temperature range, we have fitted the IPC data to a simple multitemperature (6-T) model with a temperature distribution of $\log_{10} T(\mathrm{K}) = 5.4$, 5.6, 5.8, 6.0, 6.3, and 6.6. In this model, the fractional contribution to the emission measure by each temperature component was one-sixth of the total. The fitted spectra for the isothermal and 6-T models are compared in Figures 10 and 11 for β Cen A and

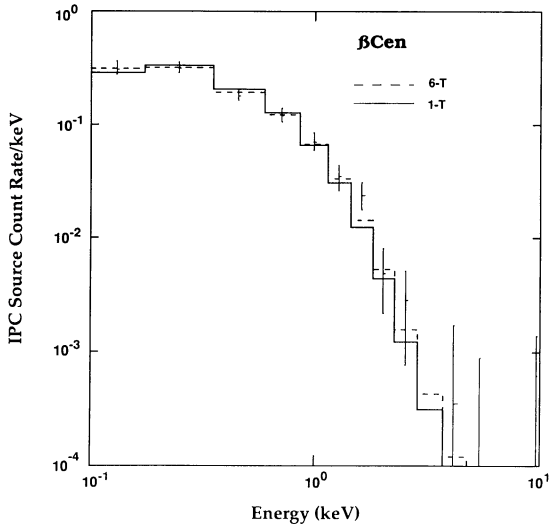

FIG. 10.—Comparison of isothermal (*solid curve*) and 6-T (*dashed curve*) fits to the IPC data (*error bars*) for β Cen A.

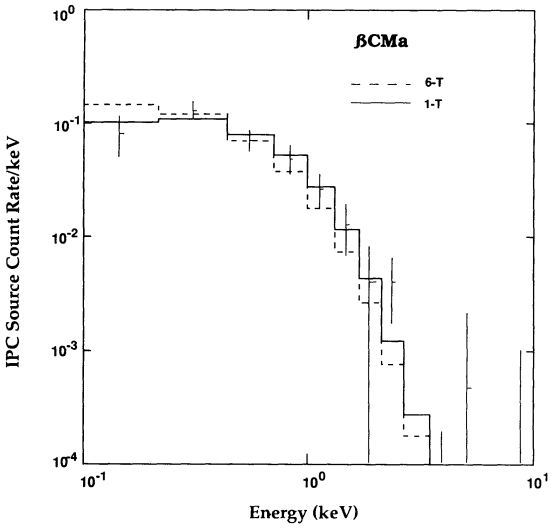

FIG. 11.—Same as Fig. 3, but for β CMa.

β CMa, respectively. Results for the emission measure and χ^2 for the best-fit cases are tabulated in Table 5. Note that the fits for this very simple 6-T model are reasonably good, with the χ^2 values being roughly similar to those for the single-temperature fits. Surely, one could obtain better multi-temperature fits to the IPC data by adjusting the relative contribution of the different temperature components to the total emission measure. We do not wish to argue here that one model is better than the other. Rather the point we wish to emphasize here is that *the X-ray emitting regions may very well have a wide range of temperatures.* Unfortunately, the IPC data alone does not provide significant constraints on the temperature distributions of the X-ray emitting regions of hot stars. This also means that the velocity jumps at the shock fronts are not significantly constrained.

4.2. *Predicted EUVE Spectra*

Significantly better constraints for the properties of hot star extended atmospheres may come from observations with *EUVE*. The *EUVE* spectrometers have a spectral resolution ($\lambda/\Delta\lambda$) of about 250–350 in the wavelength region between 70 and 700 Å (Hettrick et al. 1985; Welsh et al. 1990). This should enable the fluxes from individual lines to be measured, thereby providing significant temperature constraints for X-ray emitting plasmas. For example, Figures 12 and 13 show for β CMa and α Vir, respectively, the simulated spectra for the *EUVE* spectrometers for the isothermal and 6-T models described above. To compute the spectra, we calculated line fluxes for the 1-T and 6-T models using the Raymond-Smith code and fed the results through an *EUVE* spectrum simulation program. The ISM column densities listed in Table 3 were used to compute the attenuated EUV line fluxes. (For β CMa, the upper limit was used.) For β CMa it is seen that the isothermal

TABLE 5

MULTITEMPERATURE (6-T) FITS TO IPC DATA

Star	IPC Bins	EM (cm^{-3})	χ^2
β CMa	1–8	4.3×10^{53}	8.6
α Vir	1–8	2.6×10^{53}	7.1
β Cen A	1–9	2.6×10^{53}	3.4

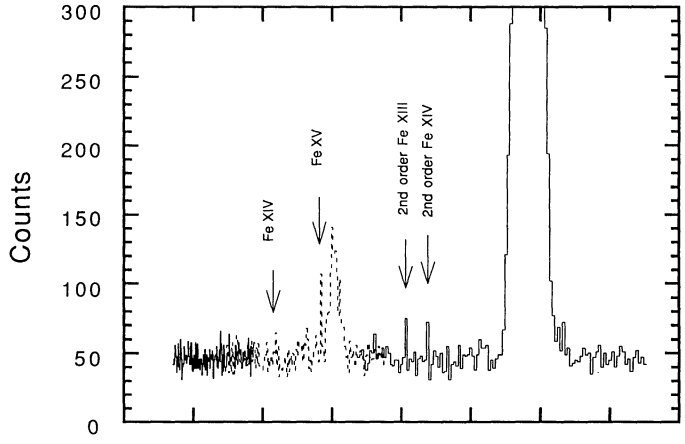

FIG. 12*a*

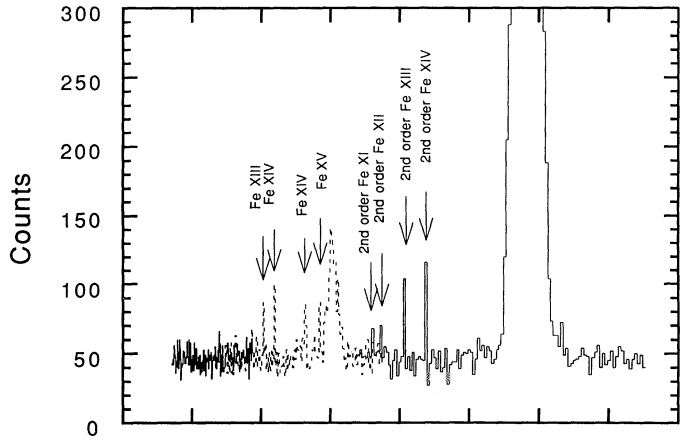

FIG. 12*b*

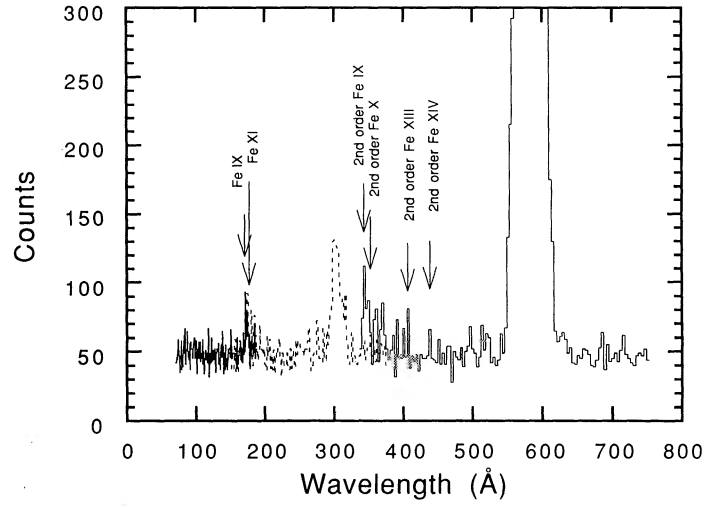

FIG. 12*c*

FIG. 12.—Simulated *EUVE* spectral response for β CMa: (*a*) isothermal model with $T = 10^{6.4}$ K, EM = 3.0×10^{53} cm^{-3}; (*b*) isothermal model with $T = 10^{6.3}$ K, EM = 2.2×10^{53} cm^{-3}; (*c*) 6-T model. The midwavelength spectrometer response (*dashed line*) separates the short- and long-wavelength spectrometer contributions (*solid lines*). The wide peaks near 304 and 584 Å are due to geocoronal He lines. Line identifications are taken from Raymond & Smith (1977).

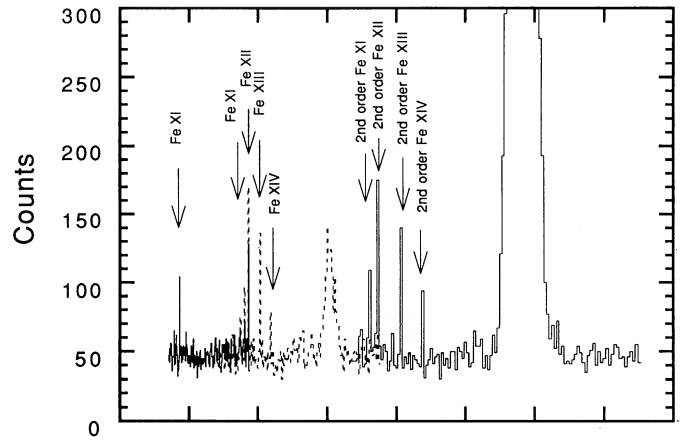

FIG. 13*a*

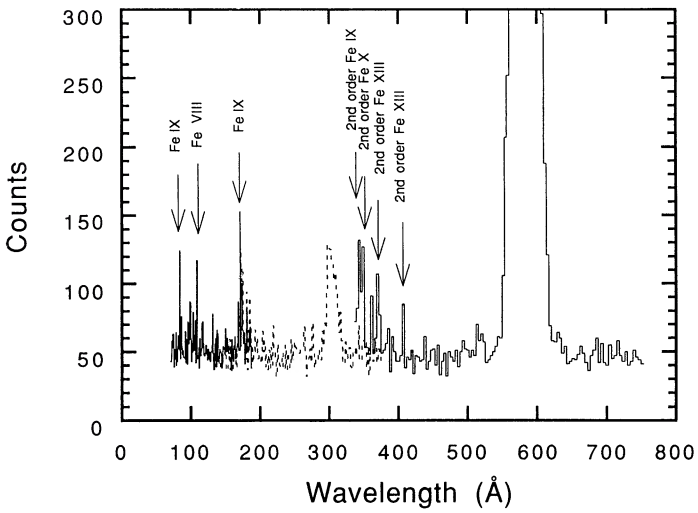

FIG. 13*b*

FIG. 13.—Simulated *EUVE* spectral response for α Vir: (*a*) isothermal model with $T = 10^{6.2}$ K, EM = 1.1×10^{53} cm^{-3}; (*b*) 6-*T* model. The mid-wavelength spectrometer response (*dashed line*) separates the short- and long-wavelength spectrometer contributions (*solid lines*). The wide peaks near 304 and 584 Å are due to geocoronal He lines. Line identifications are taken from Raymond & Smith (1977).

best fit case ($T = 10^{6.4}$ K, EM = 3.0×10^{53} cm^{-3}) shows marginal detection of lines. The *EUVE* spectrum from another plausible isothermal model which provides a reasonable fit to the IPC spectrum is shown in Figure 12*b*. This corresponds to a case in which $T = 10^{6.3}$ K, EM = 2.2×10^{53} cm^{-3}, and $\chi^2 = 10.8$. In this case, several strong lines are more readily seen at $\lambda > 200$ Å. Our results show that the line fluxes are clearly model-dependent, with the emission being near the limit of the minimum detectable flux for the *EUVE* spectrometers.

Figure 13*a* shows that for α Vir an isothermal plasma region with a temperature of $T = 1.6 \times 10^6$ K and EM = 1.1×10^{53} cm^{-3} would be detected by the short- and midwavelength *EUVE* spectrometers. Several iron lines from ionization stages Fe XI through Fe XIV should have measurable fluxes. Second-order photons (at $\lambda = 2\lambda_{\rm line}$) are detected by the long-wavelength spectrometer.

Figures 12*c* and 13*b* show simulated *EUVE* spectra for the 6-*T* plasma model. Table 6 lists the ions that are present and

TABLE 6

OBSERVABLE EUV LINES

Wavelength (Å)	Ion	log T_{max}
83.45	Fe IX	6.0
86.77	Fe XI	6.0
108.1	Fe VIII	5.8
171.1	Fe IX	5.8
174.6	Fe X	6.0
180.4	Fe XI	6.0
185.2	Fe VIII	5.8
186.9	Fe XII	6.2
203.8	Fe XIII	6.2
219.1	Fe XIV	6.2
264.5	Fe XIV	6.2
284.2	Fe XV	6.4

the temperature component giving the greatest contribution for each line. In both cases, lines are observed between 80 and 500 Å. Note that again Fe lines are the most readily observable. Several EUV lines originate in the lower temperature components of the plasma. These components contribute little to the X-ray flux, but will produce strong emission lines at EUV wavelengths.

We have also calculated the emission for both the isothermal and multitemperature models for β Cen. Because of the relatively high ISM column density, the predicted EUV fluxes are slightly below the detection threshold of the *EUVE* spectrometers.

It is not clear if there is a significant amount of "warm" material (10^5 K $< T < 10^6$ K) in the winds of early B stars. Although plasmas in this temperature range tend to cool radiatively much faster than higher temperature plasmas, the densities of B star winds may be low enough that cooling times become long. For τ Sco, radiative cooling was found to be important for shocks forming close to the star (MC). However, it seems possible that warm material could exist farther from the star, where densities are lower and cooling times are longer. If β CMa has a significant amount of warm material in its wind—i.e., comparable to the amount of material producing its X-ray luminosity—*EUVE* should be able to detect the lines emitted from this lower temperature plasma.

5. CONCLUSIONS

We have shown that observations of the EUV line emission from nearby early B stars can lead to a significant improvement in our understanding of their X-ray source properties. We have examined the line emission from a narrow spectral band (100 Å $< \lambda <$ 110 Å) to show the dependence of the EUV line spectrum on the temperature of the X-ray-emitting region. In addition, spectral analysis of the line profiles could allow one to definitively determine whether the X-rays are produced by a corona at the base of the wind or by shocks embedded in the wind. Because a corona at the low-velocity base of the wind would emit lines which are relatively narrow. Lines emitted from shock-heated plasmas embedded in the wind would exhibit rather broad profiles resulting from Doppler broadening. The detection of individual emission lines by moderate-resolution spectrometers, such as those on *EUVE*, could provide valuable constraints on the temperature distributions throughout the X-ray emitting regions.

The ratio of redshifted to blueshifted intensities for each line is predicted to increase as a shock propagates out through the wind. Because of this, one could observe time-dependence, and

perhaps periodicity, in these intensity ratios. In addition, the rate of change of the red-to-blue intensity ratio would be different for lines of different wavelengths. As the shock propagates outward through the wind, the red/blue intensity ratios of lines which are most sensitive to the overlying wind column density—i.e., the lines at longer wavelengths—will change more rapidly with time. Thus, in addition to providing insights into the temperature distribution, observing a number of lines over a range of EUV wavelengths will provide more rigorous constraints for shock models.

Finally, we note that the predicted line fluxes for the stars which we consider to be the best candidates for detection are only slightly above the minimum detectable line flux of the *EUVE* spectrometers. Because of the many uncertainties involved—such as atomic data, elemental abundances, ISM and wind column densities—one cannot predict with certainty that lines will be detected by the *EUVE* spectrometers. However, with the next generation of higher-resolution, more sensitive EUV spectrometers, such as that to be flown on the ORFEUS/SPAS mission (Hurwitz & Bowyer 1990), the effects predicted in this paper should be observable.

The authors gratefully acknowledge F. R. Harnden's assistance in obtaining the *Einstein* IPC data. We thank H. Lamers for valuable comments concerning this paper, J. J. M. and J. P. C. are supported in part by NASA grant NAGW-2210. B. Y. W., P. W. V., and J. V. V. thank the *EUVE* Science Team for their advice and are supported in part by NASA Contract NAS5-30180 administered by the Space Sciences Laboratory at the University of California, Berkeley. W. L. W. is supported in part by NASA grant NAS5-30773. Computing support has been provided in part by the National Science Foundation through the San Diego Supercomputer Center.

REFERENCES

Agrawal, P. C., Singh, K. P., Riegler, G. R., & Stern, R. A. 1984, MNRAS, 208, 845
Baade, D., & Lucy, L. B. 1987, A&A, 178, 213
Bowyer, S., & Malina, R. F. 1991, in *Extreme Ultraviolet Astronomy*, ed. R. F. Malina & S. Bowyer (New York: Pergamon), 397
Cassinelli, J. P. 1985, in The Origin of Nonthermal Heating/Momentum in Hot Stars, ed. A. B. Underhill & A. G. Michalitsionos (NASA Conf. Pub. 2358), 2
Cassinelli, J. P., MacFarlane, J. J., Welsh, B., Vallerga, J., & Veddar, P. 1991, in Extreme Ultraviolet Astronomy, ed. R. F. Malina & S. Bowyer (New York: Pergamon), 153
Cassinelli, J. P., & Olson, G. L. 1979, ApJ, 229, 304
Cassinelli, J. P., & Swank J. H. 1983, ApJ, 271, 681
Cassinelli, J. P., Waldron, W. L., Sanders, W. T., Harnden, F. R., Rosner, R., & Vaiana, G. S. 1981, ApJ, 250, 677
Castor, J. I., Abbott, D. C., & Klein, R. I. 1975, ApJ, 195, 157 (CAK)
Chen, W., & White, R. L. 1991, ApJ, 366, 512
Collura, A., Sciortino, S., Serio, S., Vaiana, G. S., Harnden, F. R., & Rosner, R. 1989, ApJ, 338, 296
Gathier, R., Lamers, H. J. G. L. M., & Snow, T. P. 1981, ApJ, 247, 173
Groenewegen, M. A. T., Lamers, H. J. G. L. M., & Pauldrach, A. W. A. 1989, A&A, 221, 78
Harnden, F. R., et al. 1979, ApJ, 234, L51
Henrichs, H., Kaper, L., & Zwarthoed, G. A. 1988, in A Decade of UV Astronomy with the *IUE* Satellite, ed. E. Rolfe (ESA SP-281, Vol. 2), 145
Hettrick, M., Bowyer, S., Malina, R. F., Martin, C., & Mrowka, S. 1985, Appl. Optics, 24, 1737
Hurwitz, M., & Bowyer, S. 1990, in IAU Colloquium 123, Observatories in Earth Orbit and Beyond, ed. Y. Kondo, in press
Kaper, L., Henrichs, H. F., Zwarthoed, G. A., & Nichols-Bohlin, J. 1989, in Proc. NATO Advanced Research Workshop on Angular Momentum and Mass Loss for Hot Stars, ed. L. A. Willson & R. Stalio (Dordrecht: Kluwer), 213
Kudritzki, R. F. 1991, in Extreme Ultraviolet Astronomy, ed. R. F. Malina & S. Bowyer (New York: Pergamon), 130
Kudritzki, R. P., Pauldrach, A., Puls, J., & Abbott, D. C. 1989, A&A, 219, 205
Lamers, H. J. G. L. M., Gathier, R., & Snow, T. P. 1980, ApJ, 242, L33
———. 1982, ApJ, 258, 186
Lamers, H. J. G. L. M., & Morton, D. 1976, ApJS, 32, 715
Lamers, H. J. G. L. M., van de Heuvel, & Petterson, J. 1976, A&A, 49, 327
Lamers, H. J. G. L. M., Waters, L. B. F. M., & Wesselius, P. R. 1984, A&A, 134, L17
Long, K. S., & White, R. L. 1980, ApJ, 239, L65
Lucy, L. B. 1982, ApJ, 255, 286
Lucy, L. B., & Solomon, P. M. 1970, ApJ, 159, 879
MacFarlane, J. J., & Cassinelli, J. P. 1989, ApJ, 347, 1090, (MC)
Mihalas, D. 1978, Stellar Atmospheres, Second Edition (New York: Freeman)
Mullan, D. J. 1984, ApJ, 283, 303
Nordsieck, K. H., Cassinelli, J. P., & Anderson, C. M. 1981, ApJ, 248, 678
Owocki, S. P. 1991, in Stellar Atmospheres: Beyond Classical Models, ed. I. Hubeny & L. Crivellari (Dordrecht: Kluwer)
Owocki, S. P., Castor, J. I., & Rybicki, G. B. 1988, ApJ, 335, 914 (OCR)
Pauldrach, A. 1987, A&A, 183, 295
Pollack, A. M. T. 1987, A&A, 171, 135
Prinja, R. K. 1988, MNRAS, 231, 21
Prinja, R. K., Howarth, I. D., & Henrichs, H. F. 1987, ApJ, 317, 389
Raymond, J. C., & Smith, B. W. 1977, ApS, 35, 419
Reilman, R. F., & Manson, S. T. 1979, ApJS, 40, 815
Shull, J. M., & Van Steenberg, M. E. 1985, ApJ, 294, 599
Snow, T. P., & Morton, D. C. 1976, ApJS, 33, 269
Swank, J. H. 1985, in The Origin of Nonthermal Heating/Momentum in Hot Stars, ed. A. B. Underhill & A. G. Michalitsionos (NASA Conf. Pub. 2358), 86
Tucker, W. H., & Gould, R. J. 1966, ApJ, 144, 244
Waldron, W. L. 1984, ApJ, 282, 256
Welsh, B. Y., Vallerga, J. V., Jelinsky, P., Vedder, P. W., Bowyer, S., & Malina, R. F. 1990, Opt. Engineering, 29, 752
Welsh, B. Y., Vedder, P. W., & Vallerga, J. V. 1990, ApJ, 358, 473
Wolfire, M. G., Waldron, W. L., & Cassinelli, J. P. 1985, A&A, 142, L25